ARTICLE

Acoustofluidics for simultaneous droplet transport and centrifugation facilitating ultrasensitive biomarker detection

Received 00th January 20xx,
Accepted 00th January 20xx

DOI: 10.1039/x0xx00000x

Jingui Qian[a‡], Huaize Lan[a‡], Liang Huang[a], Shaohui Zheng[b], Xufeng Hu*[a], Minhui Chen*[b], Joshua E.-Y. Lee[c] and Wei Zhang*[d]

Trace biological sample detection is critical for the analysis of pathologies in biomedicine. Integration of microfluidics manipulation techniques typically strengthens biosensing performance. For instance, using isothermal amplification reactions to sense trace miRNA in peripheral circulation lacks a sufficiently complex pretreatment process that limits the sensitivity of on-chip detection. Herein we propose an orthogonal tunable acoustic tweezer (OTAT) to simultaneously actuate the transportation and centrifugation of μ-droplets on a single device. The OTAT enables diversified modes of droplet transportation such as unidirectional transport, multi-direction transport, round-trip transport, tilt angle movement, multi-droplet fusion, and continuous centrifugation of the dynamic droplets simultaneously. The multiplicity of modalities enables the focusing of a loaded analyte at the center of the droplet or constant rotation about the center axis of the droplet. We here demonstrate the OTAT's ability to actuate transportation, fusion, and centrifugation-based pretreatment of two biological sample droplets loaded with miRNA biomarkers and multiple mixtures, as well as facilitating the increase of fluorescence detection sensitivity by an order of magnitude compared to traditional tube reaction methods. The results herein demonstrate the OTAT-based droplet acoustofluidic platform's ability to combine a wide range of biosensing mechanisms and provide a higher accuracy of detection for one-stop point-of-care disease diagnosis.

1. Introduction

The integration of microfluidics and biosensing technologies has the potential to advance the quality of healthcare through point-of-care (POC) disease diagnosis. Several lab-on-a-chip (LOC) microfluidic diagnostic platforms have been developed to improve biosensing performance.[1] For example, the detection of miRNA in peripheral circulation has been recognized as a promising strategy for early disease diagnosis or monitoring of therapeutic response. Existing methodologies mostly rely on isothermal amplification reactions for miRNA detection without thermocycling equipment. Nevertheless, such samples still need to undergo complicated pretreatment procedures (e.g., manual mixing intensity enhancement) to capture trace concentrations of miRNA biomarkers in bodily fluids. This inevitably requires microfluidics to improve the sensitivity of miRNA detection and achieve a one-stop biosensing platform.

Microfluidics is now able to perform a range of functions in the fields of chemical analysis[2, 3] and biological detection,[4-8] such as organismal body analysis,[9] drug encapsulation,[10] cell encapsulation,[11] cell screening and sequencing,[12] and nebulizer treatment,[13] etc. Among these examples, microfluidics has demonstrated the ability to manipulate individual droplets and micro to nano-objects in liquids, enabled by various forces associated with magnetics,[14] optical,[15] acoustics,[16, 17] electrowetting-on-dielectrics, dielectrophoresis, and hydrodynamics. Acoustic tweezers based on bulk acoustic waves (BAWs)[18] and surface acoustic waves (SAWs)[19, 20] allow for on-chip micro-manipulation that is contactless,[21] non-invasive,[22] and highly biocompatible[23]. Given these unique advantages, acoustic tweezers have become a highly promising manipulation method and could play a crucial role in biomedical detection.

Droplet acoustofluidics, based on single or multiple droplet samples, allows for reduced sample requirement, reduced cost, rapid response,[24] high reproducibility, and high throughput. Typically, acoustic streaming is employed for programmable droplet manipulation[25] (i.e., merging, splitting, and mixing) with a layer of oil coating on the surface of the piezoelectric substrate.[26] Moreover, on a bare piezoelectric substrate, coupling the SAWs and radiated acoustic pressure gradient inside the droplets delivers satisfactory droplet handling within a compact footprint for module integration,[27, 28] which is highly attractive for a wide range of LOC biological applications.[29] More advanced acoustic device designs, such as a phased array ultrasonic tweezer, have been proposed for versatile droplet manipulation on superhydrophobic surfaces by adjusting the position of the focal point (e.g., using a twin trap ultrasonic

[a] Anhui Province Key Laboratory of Measuring Theory and Precision Instrument, School of Instrument Science and Opto-Electronics Engineering, Hefei University of Technology, Hefei 230009, China. E-mail: xuefeng.hu@hfut.edu.cn
[b] School of Medical Imaging, Xuzhou Medical University, Xuzhou 221006, China E-mail: minghuiai@xzhmu.edu.cn
[c] School of Electrical and Data Engineering, University of Technology Sydney, Ultimo, NSW 2007, Australia
[d] School of Physics and Optoelectronic Engineering, Guangdong University of Technology, Guangzhou 510006, China. E-mail: zhangw0520@gdut.edu.cn
Electronic Supplementary Information (ESI) available. See DOI: 10.1039/x0xx00000x
‡These authors contributed equally to this work.

field)[30]. However, it is unclear if these methods can be integrated with other essential biological sample processing capabilities, such as droplet centrifugation for reagent mixing, concentration, or purification.

Typically, different designs of interdigital transducers (IDTs) are used to generate different functions of acoustofluidic manipulation on droplets and the micro-objects contained within. The droplet acts as a carrier and is commonly used to carry biological cells,[31] proteins,[32] and other tissues in the droplet acoustofluidic platforms. The ability to transport droplets to predetermined locations quickly is critical for biochemical analysis.[33] Meanwhile, droplet centrifugation is also an essential sample preparation procedure in biological detections. Droplet centrifugation, driven by an asymmetric acoustic field, promotes adequate mixing of low-concentration analytes (e.g., trace biomarkers) inside the droplet, which helps to increase the detection sensitivity of biological samples.[34-36] Therefore, realizing both micro-droplet transportation and centrifugation simultaneously on a single acoustofluidic device could pave the way towards on-chip ultrasensitive trace biomarker detection (e.g., detection of miRNA).

In this work, we propose an orthogonal tunable acoustic tweezer (OTAT) to dynamically actuate both micro-droplet transportation and centrifugation on a single SAW device. The OTAT comprises two pairs of slanted-IDTs (SIDTs) in the X and Y directions that generate narrow acoustic beams that propagate forward toward a specific location. The analyte-containing droplet moves on the hydrophobic surface in two dimensions, driven by traveling SAWs (TSAWs) of a specific frequency. This enables several different functions such as unidirectional transport, multi-direction transport, round-trip transport, tilt angle movement, and multi-droplet fusion. Simultaneously, the droplets continue to centrifuge during this dynamic movement (as opposed to a sessile droplet), either focusing the larger analytes (>2 μm) to the center area or constantly rotating smaller analytes (0.5-2 μm) about the center axis of the droplet. We demonstrate the capabilities of the OTAT for actuating the biological sample droplet (e.g., loading biomarkers and amplification reaction mixtures) for droplet transport, fusion, and centrifugation-based pretreatment, which facilitates the fluorescence detection sensitivity of miRNA increased by an order of magnitude (from 10^{-12} M to 10^{-13} M) compared to traditional tube reaction methods. Therefore, the OTAT-based droplet acoustofluidic platform can be integrated with biosensing, promoting the accuracy and portability of POC disease diagnosis.

2. Materials and Methods

2.1 Design and fabrication of the OTAT

A schematic diagram of the OTAT is shown in Fig. 1(a). The device integrates both droplet transport and centrifugation functions. The acoustic device consists of two sets of SIDTs formed on a 128° YX $LiNbO_3$ substrate along the X and Y directions, annotated as SIDT-1, SIDT-2, SIDT-3, and SIDT-4 respectively. Each SIDT consists of 20 pairs of working electrodes with 10 pairs of reflectors that guide the TSAWs to travel in one direction to reduce dissipation of acoustic energy. The SIDT pattern was formed by lithography, followed by depositing a 300 nm thick Al layer on the $LiNbO_3$ surface using thermal evaporation. An optical image of the fabricated OTAT is displayed in Fig. 1(b). The widths and space of the electrodes and the reflectors increase from 50 μm to 100 μm, modulating the working frequency range in the X and Y directions ranges to lie within 10-20 MHz and 15-30 MHz, respectively (see S1). Before commencing the experiments, a droplet of homemade silicone polymer solution was uniformly coated and air-dried on the delay line area (e.g., manipulation region) to produce a hydrophobic and oleophobic surface to create a droplet contact angle of 100° (see S2 of ESI). The price of a quarter of a four-inch $LiNbO_3$ wafer is about 10 USD, with further reductions in cost expected with mass prodfuction. Moreover, the OTAT can be reused after careful washing using 75% alcohol solution or acetone.

2.2 Sample preparation

To characterize the effect of particle diameter on the acoustically-driven centrifugation-based enrichment efficiency, 10 different sizes of polystyrene (PS) particles (100 nm, 500 nm, 800 nm, 1 μm, 2 μm, 5 μm, 9 μm, 13 μm, 15 μm, and 20 μm) were each diluted to 4% (v/v) in deionized water (DW) as sample solutions. A portion of PS particles with a diameter of 9 μm was diluted to 2% in DW as a sample solution for the droplet transport demonstrations. During the biomarker detection experiment, we performed the "invading stacking primer" (IS-primer) amplification reaction (ISAR) in the tubes first as the control experiment. Next, we carried out the ISAR in a 16.5 μL droplet after mixing two sample droplets that include a 1.5 μL droplet containing miRNA (i.e., prepared at different concentrations) and a 15 μL droplet containing the amplification reaction mixtures (AR-mixtures). The prepared AR-mixtures consisted of 1 μL of 10 mM dNTPs, different amounts of polymerase and primer, different amounts of hairpin DNA probe (hDNA), phosphate buffer saline (PBS), and 1×Cutsmart reaction buffer. The detailed sample preparation process is discussed in S3. Thereafter, a 1.5 μL droplet of miRNA was actuated by the OTAT to move and fuse with a 15 μL droplet of AR-mixtures, which was then acoustically centrifugated for enhanced on-chip detection demonstration.

2.3 Experimental setup

To confirm the working frequency range, the four SIDTs were characterized by a network analyzer (T5260C, TRANSCOM INSTRUMENTS, Shanghai, China). To actuate the TSAWs on the $LiNbO_3$ substrate, the RF signal applied on the SIDTs was generated by a signal generator (DG4102, RIGOL, Beijing, China) and then amplified by power amplifiers (ZHL-5W-1+, Mini-Circuits, New York, USA) in conjunction with a DC power supply (GPS-2303C, GWINSTEK, Suzhou, China). The sample droplets of different volumes were pipetted (Eppendorf, 20 μL, Germany) on the top of the SAW device. The respective contact angles of

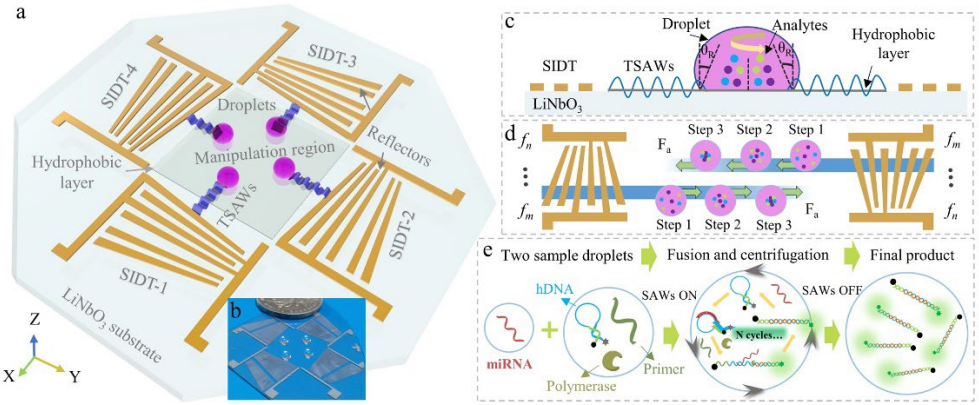

Fig. 1 Design of the OTAT for integrating droplet transport and centrifugation functions on a single acoustic device. (a) Schematic diagram of the OTAT, which consists of two sets of SIDTs patterned along the X and Y direction of a $LiNbO_3$ substrate. (b) Optical image of the fabricated OTAT. (c) Propagation of TSAWs on the surface of $LiNbO_3$ substrate and into the droplet, where θ_R is the Rayleigh angle. (d) Schematic diagram of the process of droplet transport accompanied by centrifugation for particle handling. (e) Schematic diagram of trace miRNA detection process. Small droplets loaded with miRNA biomarkers were transported and fused with larger droplets loaded with AR-mixtures, followed by droplet centrifugation to enhance the adequacy of the ISAR.

sessile droplets were derived by contact angle measuring instruments (OCA 15EC, Dataphysics, Germany). Droplet behaviors were recorded by video microscopy (AO-HD206, AOSVI, Shenzhen, China) and illuminated by an external LED to minimize light reflection. After the ISAR experiment, the irradiating fluorescence of the reacted droplets was visualized under violet light at a wavelength of 365 nm (WFH-204BS, Qiwei, Hangzhou, China). Afterward, all the reacted droplets were aspirated and sent to a multi-mode microplate reader (SpectraMax i3x, Molecular Devices, USA) to measure the specific fluorescence intensity value for miRNA biomarkers detection.

3. Working principle

As explained in Fig.1(c) and (d), the narrow beam of TSAWs excited by the SIDTs radiates along the surface of the $LiNbO_3$ substrate from the periphery of the droplet into its interior at the Rayleigh angle. When the laterally asymmetric TSAWs (i.e., asymmetric acoustic force F_a acting on the droplet) meet the droplet, a strong acoustic streaming force (ASF) will form inside the droplet to actuate the analytes in the droplet, resulting in particle enrichment at the center of the droplet or constant rotation about the center axis of the droplet due to differences in the acoustic radiation force (ARF) acting on the analytes in relation to the particle diameter. Simultaneously, the interior acoustic pressure also actuates the droplet to move forward (i.e., where the wavelengths of the TSAWs are much smaller than the size of the droplet).[24, 27, 28, 37] After initial actuation, the excitation signal frequency may be further fine-tuned to shift the propagation paths of the TSAWs for centrifugation to enhance the agglomeration of particles if needed.[38] The simulations in Fig.2(a) and (b) compare the acoustic field distribution formed by the interference of TSAWs generated by a normal IDT vs. a narrow IDT (mimicking the effect of SIDTs excited by a single given frequency). The TSAWs in the X and Y directions generated by normal IDTs interfere with each other to generate a periodic distribution of wave peaks and troughs. In contrast, the two directions of TSAWs generated by narrow IDTs form an irregular acoustic field distribution, which enables simultaneous manipulation of the droplet in two dimensions. Fig. 2(c) and (d) simulate narrow beam TSAWs (generated in relation to Fig. 2(b) propagating on the surface of the $LiNbO_3$ substrate and penetrating into the hydrophobic layer (i.e., silicon polymer analogs were used in the simulation) to form asymmetric acoustic pressure gradients inside the droplet, thus enabling both particle centrifugation and transport.[39] Therefore, the simulation results corroborate the working mechanism of the OTAT and confirm the feasibility of acoustofluidic manipulation (documented in Video S1).

The amount of miRNA expression levels in bodily fluid has critical effects across various biological processes including various pathological states. As one kind of strand displacement amplification reaction,[40] ISAR[41-43] would be applied to transform one miRNA into an abundance of fluorescent signals by opening the hairpin DNA (hDNA) at a constant temperature, which is termed the target-introducing "fuels-loading" mechanism. A schematic diagram for the simultaneous actuation of droplet

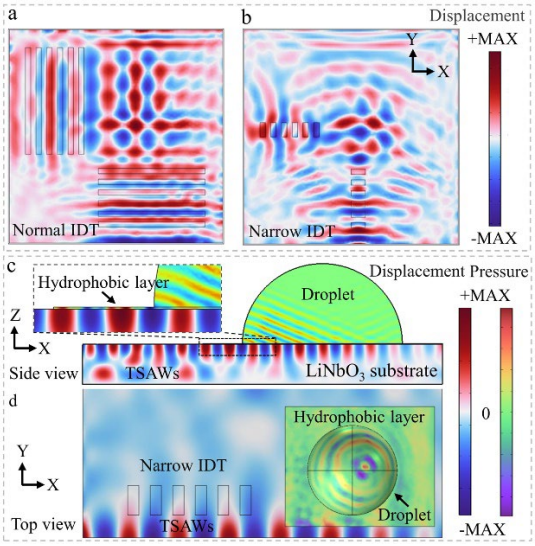

Fig. 2 Acoustic pressure distribution simulation on the $LiNbO_3$ substrate and μ-droplet. (a) and (b) acoustic field distributions formed by simultaneous excitation of TSAWs in the X and Y directions using normal IDTs and narrow IDTs (mimicking the effect of SIDTs driven at a single frequency), respectively. (c) and (d) Side view and top view of the simulation showing asymmetric TSAWs generated and propagating on the surface of the $LiNbO_3$ substrate along with the resulting acoustic field distributions inside the droplet.

transport and centrifugation with the goal of enhancing the sensitivity of trace miRNA biomarker detection is shown in Fig. 1(e). We prepared two sample droplets: a smaller droplet of miRNA biomarkers and a larger droplet compromising AR-mixtures. The smaller droplet was first actuated to move and fuse with the larger droplet. This was then followed by centrifugation of the fused droplet to enhance the adequacy of ISAR, validated by a tenfold increase in fluorescence detection sensitivity after acoustic treatment.

4. Experimental results

4.1 Effect of different volumes and power on droplet transportation

Transporting different volumes of droplets is a crucial ability for the OTAT. We applied an alternating current (AC) signal with a power of 36.5 dBm (±0.5 dBm) on SIDT-1(i.e., along the X direction). The initial excitation frequency was determined by observing the dynamics of the droplets instantaneously captured by the TSAW. The signal frequency was swept depending on the position of the droplet (e.g., between 11-15MHz). Four different volumes of droplets (1μL, 3 μL, 5 μL, and 8 μL) were successfully transported from one side of the manipulation area to the other (Fig. 3(a) and Video S2). Similarly, applying the same AC signal on SIDT2 (i.e., along the Y direction) and sweeping the excitation frequency (e.g., between 16-20 MHz) results in the same four different volumes of droplets moving the same distance but at higher speeds (Fig. 3b and Video S2). Therefore, these results validate the ability of long-distance transport of μ-droplets using the OTAT.

We have also measured the transport velocity of droplets under different levels of excitation power at the same given frequency. A 2 μL droplet was transported after applying excitation signals of 12.4 MHz (±0.2 MHz) on SIDT-1 and 20 MHz (±0.2 MHz) on SIDT-2. As shown in Fig. 4 (a), when the power was increased from 30 dBm to 37.5 dBm, the transport velocity of droplets was increased notably from about 0.2 mm/s to 2.8 mm/s in the X direction and from 0.9 mm/s to 19.5 mm/s in the Y direction. The results indicate that the transport velocities of droplets in both directions differ significantly due to the anisotropy of the $LiNbO_3$ crystal. To coordinate droplet handling in different

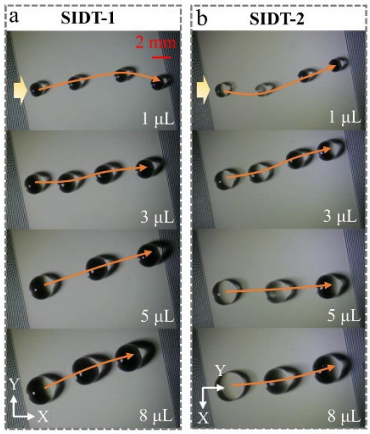

Fig. 3 Performance characterization of acoustic droplet manipulation along the X and Y directions. The transportation trajectories of four different volumes of droplets (1 μL, 3 μL, 5 μL, and 8 μL) in the X (a) and Y (b) directions, respectively.

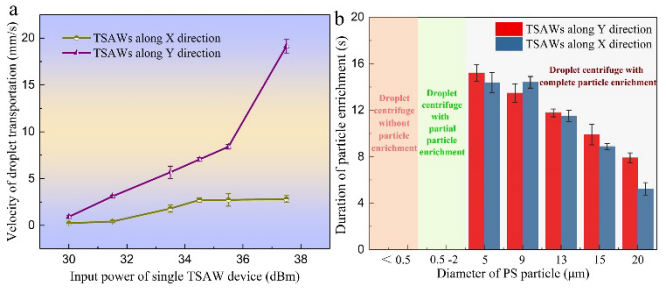

Fig. 4 Quantitative characterization of droplet manipulation and centrifugation. (a) Effect of different input powers on the transport velocity of 2 μl droplet. (b) Duration of particle enrichment of different diameters inside the droplet under the same power.

directions, the droplet velocity could be tuned by adjusting the TSAW path and the power amplitude of the excitation signal.

4.2 Effect of centrifugation on different analyte sizes

To characterize the centrifugation performance of the OTAT, we employed PS particles of different diameters (same concentration kept at 4%) serving as analytes in the experiment. We observed three classes of outcomes resulting from the same actuation condition of 20 MHz (±0.1 MHz) frequency and power of 31.5 dBm (±0.5 dBm) applied to SIDT-2 for Y direction TSAW propagation: (1) the smallest PS particles (100 nm diameter) only rotated about the center axis of the droplet instead of clustering at the center (Fig. 5a); (2) mid-sized PS particles (diameters of 500 nm, 800 nm, 1 μm, and 2 μm) both rotated and partially cluster at one side of the droplet (Fig. 5b-e); (3) the largest PS particles (diameters of 5 μm, 9 μm, 13 μm, 15 μm, 20 μm) cluster completely at one side of the droplet (Fig. 5 f-j). Fig 4(b) summarizes the enrichment time of the particles (concentration of 4%) in relation to size inside the 5 μL droplet treated by the TSAWs along X and Y directions. These results indicate that the larger the particle diameter (>5 μm), the shorter the enrichment duration, given that the ARF is proportional to the third power of particle diameter.[44, 45] The results for particles smaller than 2 μm have been omitted because there was no enrichment or the enrichment was only

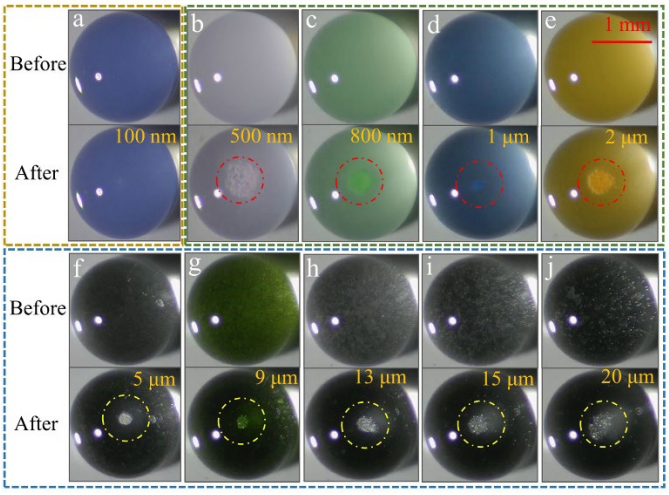

Fig. 5 Performance characterization of acoustic centrifugation for a range of particle diameters from 100 nm to 20 μm. (a) Rotation about the center of the

droplet only (yellow dotted box), partial clustering of particles (cyan dotted box), and full clustering of particles (blue dotted box).

partial and impossible to count the particles (i.e., the ARF applied to the analyte is insufficient for efficient capture due to the strong dependence of ARF on particle size). It is worth mentioning that the centrifugal function of maintaining high rotation speed or partial enrichment meets the needs for trace biomarkers (e.g. in the nanoscale range) in this work.

4.3 Diversified droplet manipulation in a single direction

The wide operating frequency range of the OTAT uniquely enables both droplet transport and centrifugation by using a single SIDT or combinations of SIDTs. We swept the frequency between 10-15 MHz for SIDT-1 (X direction) and between 19-25 MHz for SIDT-2 (Y direction) to manipulate droplets in a single direction. As shown in Fig. 6, exciting the TSAWs (e.g., the input power of 35dBm) to act at different positions along the periphery of the droplets pushes the droplets to move along different angles relative to a horizontal reference. When the path of the TSAW is aligned with the center of the droplet, the droplet moves forward and the angle between the droplet transport trajectory and the center line of the droplet is close to 0 (Fig. 6a). When the path of TSAW is below the center of the droplet, the droplet trajectory is along a positive acute angle relative to the horizontal line (+23°) (Fig. 6b). When the path of the TSAW is above the center of the droplet, the droplet trajectory is along a negative acute angle relative to the horizontal line (-13°) (Fig. 6c). Droplet transport along different angles of trajectories have been captured in Video S3. Therefore, the transmission path of TSAWs generated by the OTAT could be changed by tuning the signal frequency, thereby changing the trajectory path of droplets as desired. Quickly adjusting the excitation frequency helps to correct the droplet movement trajectory if needed. Fig. 6 (d), (e), and Video S4 demonstrate the fusion of two initially separate droplets. Actuation is applied to droplet A, which moves and fuses with stationary target droplet B in the form of offset angles relative to the horizontal reference line for both the X and Y directions

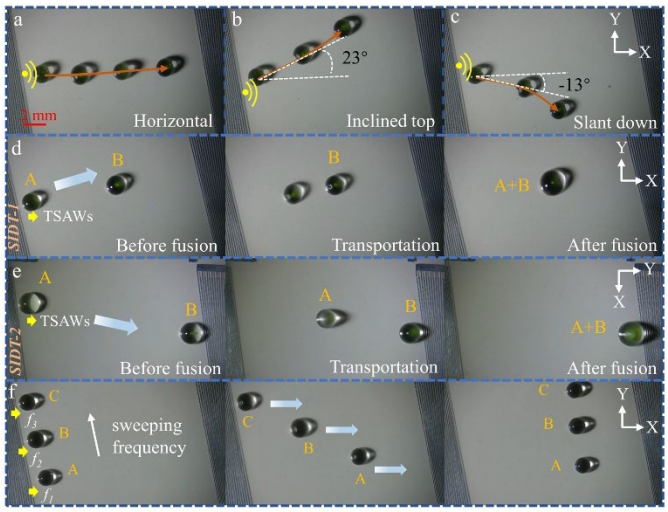

Fig. 6 Diversified droplet transport in multiple programmable directions as desired. (a), (b) and (c) Different droplet transport trajectories resulting from TSAWs acting parallel and slanted relative to the center line of the droplet. (d) and (e) Droplet A pushed to fuse with droplet B (stationary) by TSAW actuation in the X and Y direction, respectively. (f) Manipulating multiple droplets by sweeping frequency.

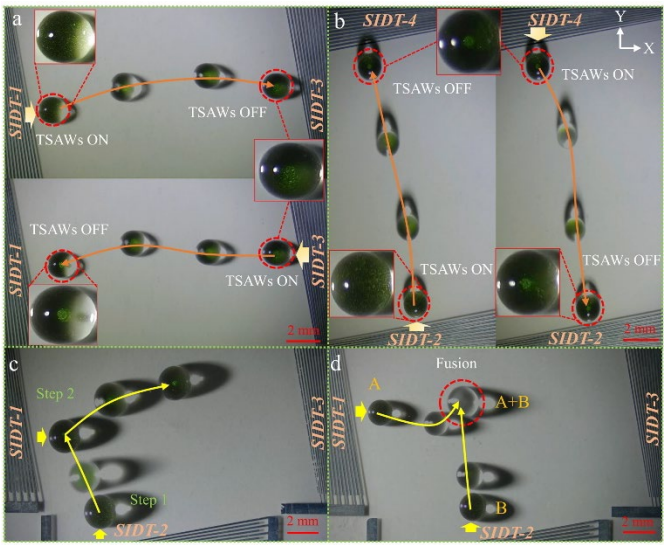

Fig. 7 Diversified droplet manipulation in multiple directions. (a) and (b) A 1 µL droplet being transported forward and backward in the X and Y directions, respectively. (c) A 2 µL droplet subjected to "right angle" transport under TSAW actuation in Y and X directions in sequence. (d) Two 1 µL droplets of pushed simultaneously towards each other and fused into one under TSAW actuation in both X and Y directions.

respectively. The stationary state of droplet B, while droplet A is actuated, is due to the partial acoustic absorption by droplet A, and the larger attenuation being at a far longer distance from the source of the TSAW.[16] Interestingly, all droplet transport processes are accompanied by droplet centrifugation. Fig. 6 (f) and Video S4 illustrate OTAT's ability to transport multiple (≥3) droplets continuously by sweeping the frequency of the SIDTs.

4.4 Diversified droplet manipulation in multiple directions

Fig. 7 illustrates how using a combination of SIDTs can manipulate droplets in a variety of modes. After applying an excitation signal with a power of 36.5 dBm (±0.5 dBm) on SIDT-1 and tuning the frequency, the droplet moved from the edge of SIDT-1 to the edge of the SIDT-3, as shown in Fig. 7(a). Apart from droplet transport, the particles clustered on the side of the droplet. Subsequently turning off SIDT-1 and turning on SIDT-3 with the same excitation signal moves the droplet back to its initial position, with the particles clustered on one side of the droplet. The same test was repeated for SIDT-2 and SIDT-4 (same power but different frequency) and similar results were recorded in Fig. 7(b). Therefore, the OTAT enables both round-trip transport of droplets as well as centrifugation by sequentially exciting TSAWs with different SIDTs in the same direction, which is also documented in Video S5.

The results show that exciting SIDTs along one axis actuate one-dimensional droplet transport. Conversely, two-dimensional droplet transport requires exciting SIDTs in both X and Y directions, as shown in Fig. 7(c) and Video S6. In these experiments, a 2 µL droplet was first placed at the edge of SIDT-2. The TSAWs generated from SIDT-2 push the droplet away from SIDT-2 and towards the edge of SIDT-1. Upon reaching the edge of SIDT-1, turning off SIDT-2 and turning on SIDT-1 pushes the droplet away from SIDT-1 to move toward the center of the manipulation region. The net effect is a curved path in the clockwise direction, or “right angle” transport. In addition, we

also used the TSAWs in the X and Y directions simultaneously to fuse two droplets in the center of the manipulated region. Two 1 µL droplets were placed on the front edge of SIDT-1 and SIDT-2. Applying an excitation signal with a power of 35 dBm and tuning the frequencies on both SIDTs transports the initially separated two droplets to the center of the manipulation region where they then fuse into a single droplet, as shown in Fig. 7 (d) and Video S7. These results indicate that the combination of four TSAWs in two directions allows for diverse manipulation of µ-droplets.

4.5 Acoustofluidic manipulation facilitates ultrasensitive miRNA detection

As mentioned earlier, fusion with microfluidic sample treatment technology will improve the sensitivity of biological detection. We have combined the acoustofluidic droplet manipulation technique with on-chip trace miRNA detection. Under the optimal conditions, five kinds of concentrations of miRNA-21 (0, 10^{-15} M-10^{-12} M) were prepared using the serial dilution method in PBS for detection to investigate the sensitivity of our OTAT treatment method (experiment group) and traditional tube reaction method (control group). We conducted the same acoustofluidic manipulation function described in Fig. 6(d) and (e). First, a smaller 1.5 µL droplet of miRNA was actuated by the OTAT to move and fuse with a larger 15 µL droplet of prepared AR-mixtures accompanied by centrifugation for 11.1 s. Next, the drive frequency was adjusted to actuate only centrifugation for about 40 s. The state of the droplets were then recorded every 5 min for the next 30 min. Every 5 min, we turned on the acoustic centrifugation for about 15 s. Recorded optical images of the droplet during the 30 min period are captured in S4. Fig. 8(a) and Video S8 record the transport and fusion of the two droplets for miRNA detection.

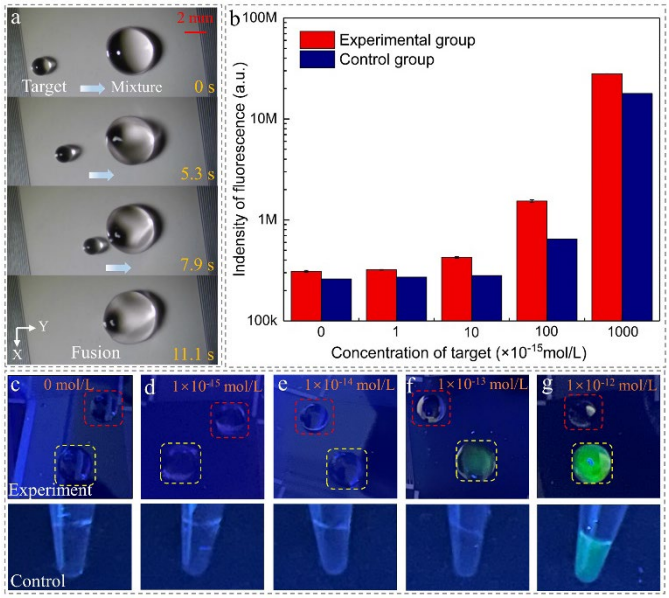

Fig. 8 Ultrasensitive detection of trace miRNA biomarkers. (a) A 1.5 µL droplet of miRNA is moved and fused with a 15 µL droplet of the AR-mixtures accompanied by centrifugation within 11.1 s. (b) Numerical fluorescence intensity of miRNA detection at five different concentrations by the OTAT treatment method and traditional tube reaction method. (c-g) Fluorescence visualization analysis of miRNA at concentrations of 0, 1, 10, 100, and 1000×10^{-15} mol/L after full reaction (experimental group) under violet light irradiation at 365 nm, respectively, which is compared with the traditional tube reaction method (control group).

The fluorescence signal intensity is determined by the number of opening hDNA, which in turn indicates the amplification efficiency of the target-introducing "fuels-loading" mechanism. The fluorescence signal from the OTAT treatment method responded with a miRNA-21 concentration of about 10^{-13} M, while the same fluorescence signal from the traditional tube reaction method responded with a miRNA-21 concentration of about 10^{-12} M as shown in Fig. 8(b). Under violet light (UV) irradiation at a wavelength of 365 nm, it can be observed that the fluorescence intensity from the "fuels-loading" mechanism (e.g., highlighted by a yellow dashed box) under droplet manipulation is significantly higher than that without "fuels-loading" (without miRNA target, e.g., highlighted by a red dashed box) as shown in Fig. 8(c-g). The red dashed box of Fig. 8(c-g) shows the negative control experiment result of miRNA-21 detection by the OTAT treatment with the same conditions, indicating this assay could provide a sensitive method without false positive results. Moreover, the OTAT can efficiently enhance the detection sensitivity of trace biomarkers by providing high-speed rotation of droplets and adequate analyte mixing to improve the probability of miRNA targets being amplified for enhanced amplification efficiency. We characterized the temperature change on the droplet during acoustic manipulation (mimicking the process of miRNA detection). As discussed in S5, the feeble thermal effect from the OTAT does not affect the detection sensitivity of miRNA biomarkers. A comprehensive comparison of recently developed droplet microfluidic technologies for miRNA detection is discussed in S6, which highlights the advantage of the OTAT in terms of both sensitivity and response time.

5. Discussion

In this work, four SIDTs were used to form an OTAT to excite a narrow beam of TSAWs, which radiates into the interior of the droplet as an asymmetric wave to actuate the droplet transport and centrifugation simultaneously. Compared with the conventional design, the OTAT simplifies the experimental operation. Integrating droplet transport and centrifugation on a single acoustofluidic device benefits analyte bioassays available in trace concentrations. In our experiments, droplets were randomly pipetted on the manipulation region and the propagation path of the TSAWs could be accurately tuned to capture the droplet by sweeping the drive frequency. We can determine whether the TSAWs have captured the droplet by observing whether the droplet shape wobbles during the frequency sweep.

However, the current state of the realized OTAT is still some way off from automation and clinical use. At present, one is unable to accurately predict and judge the excitation position of TSAWs initially. One must judge the propagation path of TSAWs by sweeping the frequency within the operating frequency of corresponding SIDTs and observing the dynamics of droplets. During the process of droplet transport with centrifugal action, the centrifugation could be unsatisfactory, requiring fine-tuning

of the exciting frequency to adjust the propagation path to enhance centrifugation results. Moreover, the treatment effect of the hydrophobic surface affects the frictional force of the droplet with the substrate surface when it slides, which will change the droplet transport trajectory (for example, becoming curved). If it is necessary to transport the droplet to a predetermined position, one could quickly adjust the excitation frequency or use multiple SIDTs in combination to reconfigure the propagation path of the TSAWs to correct the droplet trajectory. In addition, to refine the experiment and reduce droplet evaporation over longer experiment times, one could perform the assay on biological samples in an oil-phase environment (see S7). The preprocessing steps of the demonstrated miRNA detection are relatively few. As explained in S8, the proposed OTAT also has the application potential in multi-step manipulation processing for multiple droplets to facilitate miscellaneous biological detection.

6. Conclusions

We designed two pairs of orthogonal SIDTs to form an OTAT and developed a multifunctional droplet manipulation technology, which integrates droplet transportation and centrifugation on a single acoustofluidic chip. Droplet transport trajectory and centrifugation efficiency can be tuned by shifting the excitation frequency of the input signal and using different SIDTs in sequence. We used single SIDT and multiple SIDTs to realize different droplet transport trajectories and functions, such as unidirectional transportation, multi-direction transportation, round-trip transport, tilt angle movement, and multi-droplet fusion. We have shown that the OTAT is able to push larger analytes ($>$2 μm) to cluster at the droplet center while smaller analytes ($<$0.5-2 μm) remain orbited around the center axis of the droplet. This work opens new ideas about pathogen detection in the field of biology and medicine. We have demonstrated that the OTAT is capable of a successive series of pretreatment processes of droplets containing biological samples, including transport, fusion, and centrifugation, resulting in the increase in fluorescence detection sensitivity of miRNA by an order of magnitude (from 10^{-12} M to 10^{-13} M) compared to traditional tube reaction methods. These results highlight the potential of the proposed OTAT-based droplet acoustofluidic platform to be integrated with a range of biosensing techniques such as pathological cell detections, drug delivery, and biological component analysis, towards building a one-stop on-chip high-accuracy POC disease diagnostic device.

Author Contributions

Jingui Qian and Huaize Lan: writing the original draft, conceptualization, methodology, formal analysis, and data curation. Liang Huang, Shaohui Zheng, and Xufeng Hu: visualization, investigation. Minhui Chen: bio-experiment, investigation, writing-review & editing. Joshua E.-Y. Lee and Wei Zhang: funding, supervision, review & editing.

Conflicts of interest

There are no conflicts to declare.

Acknowledgments

This work was supported by the National Natural Science Foundation of China (Grant No. 62301209), the Natural Science Foundation of Anhui Province (Grant No. 2308085QF196), Anhui Science and Technology Major Project (Grant No. 202103a07020014, 202203a07020013), and the Scientific Research Project of Health Commission of Jiangsu Province (Z2022007).

Notes and references

1. S. A. N. Gowers, M. L. Rogers, M. A. Booth, C. L. Leong, I. C. Samper, T. Phairatana, S. L. Jewell, C. Pahl, A. J. Strong and M. G. Boutelle, *Lab Chip*, 2019, **19**, 2537-2548.
2. L. Shang, Y. Cheng and Y. Zhao, *Chem. Rev.*, 2017, **117**, 7964-8040.
3. R. Wang and X. Wang, *Sens. Actuators, B*, 2021, **329**, 129171.
4. D.-K. Kang, M. Monsur Ali, K. Zhang, E. J. Pone and W. Zhao, *TrAC, Trends Anal. Chem.*, 2014, **58**, 145-153.
5. Y. Ou, S. Cao, J. Zhang, W. Dong, Z. Yang and Z. Yu, *TrAC, Trends Anal. Chem.*, 2021, **143**, 116333.
6. J. Reboud, Y. Bourquin, R. Wilson, G. S. Pall, M. Jiwaji, A. R. Pitt, A. Graham, A. P. Waters and J. M. Cooper, *Proc. Natl. Acad. Sci. U. S. A.*, 2012, **109**, 15162-15167.
7. F. Liu, A. Ge, C. Li, W. Gao, F. Wu, L. Kan, J. Xu and B. Ma, *Anal. Chem.*, 2023, **95**, 6672-6680.
8. H. Hu, G. Cai, Z. Gao, C. Liang, F. Yang, X. Dou, C. Jia, J. Zhao, S. Feng and B. Li, *Analyst*, 2023, **148**, 1939-1947.
9. C. Chen, Y. Gu, J. Philippe, P. Zhang, H. Bachman, J. Zhang, J. Mai, J. Rufo, J. F. Rawls, E. E. Davis, N. Katsanis and T. J. Huang, *Nat. Commun.*, 2021, **12**, 1118.
10. Z. Wang, J. Rich, N. Hao, Y. Gu, C. Chen, S. Yang, P. Zhang and T. J. Huang, *Microsyst. Nanoeng.*, 2022, **8**, 45.
11. R. Li, Z. Gong, Z. Wu, H. Chen, Y. Xia, Y. Liu, F. Wang and S. Guo, *Nano Futures*, 2020, **4**, 045001.
12. B. Hu, P. Xu, L. Ma, D. Chen, J. Wang, X. Dai, L. Huang and W. Du, *Mar. Life. Sci Technol.*, 2021, **3**, 169-188.
13. C. Cortez-Jugo, S. Masoumi, P. P. Y. Chan, J. Friend and L. Yeo, *Ultrason. Sonochem.*, 2022, **88**, 106088.
14. D. S. Juang, J. M. Lang and D. J. Beebe, *Lab Chip*, 2022, **22**, 286-295.
15. C. Zhai, C. Hu, S. Li, Y. Ma, Y. Zhang, T. Guo, H. Li and X. Hu, *Nanoscale Adv.*, 2021, **3**, 279-286.
16. G. Destgeer, H. Cho, B. H. Ha, J. H. Jung, J. Park and H. J. Sung, *Lab Chip*, 2016, **16**, 660-667.
17. Y. Yang, Y. Yang, D. Liu, Y. Wang, M. Lu, Q. Zhang, J. Huang, Y. Li, T. Ma, F. Yan and H. Zheng, *Nat. Commun.*, 2023, **14**, 3297.
18. D. Foresti, M. Nabavi, M. Klingauf, A. Ferrari and D. Poulikakos, *Proc. Natl. Acad. Sci. U. S. A.*, 2013, **110**, 12549-12554.
19. R. Tao, G. McHale, J. Reboud, J. M. Cooper, H. Torun, J. Luo, J. Luo, X. Yang, J. Zhou, P. Canyelles-Pericas, Q. Wu and Y. Fu, *Nano Lett.*, 2020, **20**, 3263-3270.
20. X. Liu, X. Chen, Z. Yang, H. Xia, C. Zhang and X. Wei, *Sens. Diagn.*, 2023, **2**, 507-528.
21. P. Zhang, C. Chen, F. Guo, J. Philippe, Y. Gu, Z. Tian, H. Bachman, L. Ren, S. Yang, Z. Zhong, P. H. Huang, N. Katsanis, K. Chakrabarty and T. J. Huang, *Lab Chip*, 2019, **19**, 3397-3404.
22. M. Wiklund, *Lab Chip*, 2012, **12**, 2018-2028.

23. P. Vachon, S. Merugu, J. Sharma, A. Lal, E. J. Ng, Y. Koh, J. E. Lee and C. Lee, *Lab Chip*, 2023, **23**, 1865-1878.
24. R. Tao, J. Reboud, H. Torun, G. McHale, L. E. Dodd, Q. Wu, K. Tao, X. Yang, J. T. Luo, S. Todryk and Y. Fu, *Lab Chip*, 2020, **20**, 1002-1011.
25. S. P. Zhang, J. Lata, C. Chen, J. Mai, F. Guo, Z. Tian, L. Ren, Z. Mao, P. H. Huang, P. Li, S. Yang and T. J. Huang, *Nat. Commun.*, 2018, **9**, 2928.
26. P. Zhang, C. Chen, X. Su, J. Mai, Y. Gu, Z. Tian, H. Zhu, Z. Zhong, H. Fu, S. Yang, K. Chakrabarty and T. J. Huang, *Sci. Adv.*, 2020, **6**, eaba0606.
27. X. Qin, X. Wei, L. Li, H. Wang, Z. Jiang and D. Sun, *Lab Chip*, 2021, **21**, 3165-3173.
28. T. Fukaya and J. Kondoh, *Jpn. J. Appl. Phys.*, 2015, **54**, 07he06.
29. Y. Q. Fu, J. K. Luo, N. T. Nguyen, A. J. Walton, A. J. Flewitt, X. T. Zu, Y. Li, G. McHale, A. Matthews, E. Iborra, H. Du and W. I. Milne, *Prog. Mater. Sci.*, 2017, **89**, 31-91.
30. Y. Zichao, L. Chenguang, L. Cong, B. Xiangge, Z. Lei, F. Shile and L. Yahua, *Sci. adv.*, 2023, **9**, eadg2352.
31. P. K. Periyannan Rajeswari, H. N. Joensson and H. Andersson-Svahn, *Electrophoresis*, 2017, **38**, 305-310.
32. Z. Yu, J. Jin, L. Shui, H. Chen and Y. Zhu, *TrAC, Trends Anal. Chem.*, 2021, **143**, 116411.
33. W. Wei, Y. Wang, Z. Wang and X. Duan, *TrAC, Trends Anal. Chem.*, 2023, **160**, 116958.
34. G. Yuyang, C. Chuyi, M. Zhangming, B. Hunter, B. Ryan, R. Joseph, W. Zeyu, Z. Peiran, M. John, Y. Shujie, Z. Jinxin, Z. Shuaiguo, O. Yingshi, W. D. T. W, S. Yoel and H. T. Jun, *Sci. adv.*, 2021, **7**, eabc0467.
35. Z. Haodong, Z. Peiran, Z. Zhanwei, X. Jianping, R. Joseph, M. John, S. Xingyu, T. Zhenhua, B. Hunter, R. Joseph, G. Yuyang, K. Putong, C. Krishnendu, W. T. P and H. T. Jun, *Sci. adv.*, 2021, **7**, eabc7885.
36. T. Zhenhua, W. Zeyu, Z. Peiran, N. T. Downing, M. John, W. Yuqi, Y. Shujie, G. Yuyang, B. Hunter, L. Yaosi, Y. Zhiming and H. T. Jun, *Sci. adv.*, 2020, **6**, eabb0494.
37. M. Sui, H. Dong, G. Mu, J. Xia, J. Zhao, Z. Yang, T. Li, T. Sun and K. T. V. Grattan, *Lab Chip*, 2022, **22**, 3402-3411.
38. Y. Bourquin, J. Reboud, R. Wilson and J. M. Cooper, *Lab Chip*, 2010, **10**, 1898-1901.
39. H. Lan, J. Qian, Y. Liu, S. Lu, B. Zhang, L. Huang, X. Hu and W. Zhang, *Micromachines*, 2023, **14**, 837.
40. C. Shi, Q. Liu, C. Ma and W. Zhong, *Anal. Chem.*, 2014, **86**, 336-339.
41. M. Chen, R. Luo, S. Li, H. Li, Y. Qin, D. Zhou, H. Liu, X. Gong and J. Chang, *Anal. Chem.*, 2020, **92**, 13336-13342.
42. W. Liu, M. Zhu, H. Liu, J. Wei, X. Zhou and D. Xing, *Biosensors and Bioelectronics*, 2016, **81**, 309-316.
43. Y. Chang, Y. Zhuo, Y. Chai and R. Yuan, *Anal. Chem.*, 2017, **89**, 8266-8272.
44. R. Wilson, J. Reboud, Y. Bourquin, S. L. Neale, Y. Zhang and J. M. Cooper, *Lab Chip*, 2011, **11**, 323-328.
45. G. Destgeer, J. H. Jung, J. Park, H. Ahmed and H. J. Sung, *Anal. Chem.*, 2016, **89**, 736-744.